UNIVERSITY OF HELSINKI REPORT SERIES IN PHYSICS

HU-P-D138

LOCAL STRUCTURE OF WATER STUDIED BY COMPTON SCATTERING

Kim Nygård

Division of X-Ray Physics
Department of Physical Sciences
Faculty of Science
University of Helsinki
Helsinki, Finland

ACADEMIC DISSERTATION

To be presented, with the permission of the Faculty of Science of the University of Helsinki, for public criticism in Auditorium E204 of Physicum, Gustaf Hällströmin katu 2a, on April 21st 2007 at 12:15.

Helsinki 2007

Supervisors:

Prof. Keijo Hämäläinen
Department of Physical Sciences
University of Helsinki
Helsinki, Finland

Prof. Seppo Manninen
Department of Physical Sciences
University of Helsinki
Helsinki, Finland

Pre-examiners:

Prof. Malcolm J. Cooper
Department of Physics
University of Warwick
Coventry, United Kingdom

Prof. Pekka Hautojärvi
Laboratory of Physics
Helsinki University of Technology
Espoo, Finland

Opponent:

Prof. Abhay Shukla
Institut de Minéralogie et de Physique
des Milieux Condensés
Université Pierre et Marie Curie
Paris, France

Custos:

Prof. Keijo Hämäläinen
Department of Physical Sciences
University of Helsinki
Helsinki, Finland

Report Series in Physics HU-P-D138
ISSN 0356-0961
ISBN 978-952-10-3241-7 (printed version)
ISBN 978-952-10-3242-4 (pdf version)
http://www.ethesis.helsinki.fi
Helsinki University Printing House
Helsinki 2007

Preface

This thesis is based on research done at the Division of X-ray Physics, Department of Physical Sciences, University of Helsinki (Finland). The experimental work was carried out at beamlines ID15B and BL08W of the European Synchrotron Radiation Facility (ESRF, Grenoble, France) and the Super Photon Ring - 8 GeV (SPring-8, Hyogo, Japan), respectively.

I am most indebted to my supervisors, Prof. Keijo Hämäläinen and Prof. Seppo Manninen, for introducing me to the field of inelastic x-ray scattering and guiding me throughout this work. I am grateful to Dr. Mikko Hakala for invaluable discussions. I acknowledge the personnel at the ESRF and the SPring-8 synchrotron-radiation laboratories for their support. Notably, this work would not have been feasible without the help of Dr. Thomas Buslaps, Dr. Veijo Honkimäki, Dr. Masayoshi Itou, and Dr. Yoshiharu Sakurai. I am grateful to the contributing authors, and especially to Prof. Lars Pettersson, for helpful discussions.

I would like to thank the head of the department, Prof. Juhani Keinonen, for providing me the opportunity to work at the Department of Physical Sciences. The personnel at the Division of X-ray Physics is acknowledged for creating a pleasant workplace atmosphere. In particular, the diverse discussions during the (occasionally lengthy) coffee breaks and the weekly floorball games are fondly remembered. Finally, I thank my family and friends for encouragement.

This work was funded by the Academy of Finland, the Research Funds of the University of Helsinki, the National Graduate School in Materials Physics, and the Finnish Academy of Science and Letters (through the Vilho, Yrjö, and Kalle Väisälä Foundation).

K. Nygård : Local structure of water studied by Compton scattering (2007), 28 pages and appendices. University of Helsinki, Report Series in Physics, HU-P-D138.

Classification (INSPEC): A7870C, A6125E, A3520E, A7115M
Keywords: water, molecular liquids, interatomic distances and angles, Compton scattering, synchrotron radiation, density-functional theory

Abstract

This thesis presents a novel application of x-ray Compton scattering to structural studies of molecular liquids. Systematic Compton-scattering experiments on water have been carried out with unprecedented accuracy at third-generation synchrotron-radiation laboratories. The experiments focused on temperature effects in water, the water-to-ice phase transition, quantum isotope effects, and ion hydration. The experimental data is interpreted by comparison with both model computations and *ab initio* molecular-dynamics simulations. Accordingly, Compton scattering is found to provide unique intra- and intermolecular structural information. This thesis thus demonstrates the complementarity of the technique to traditional real-space probes for studies on the local structure of water and, more generally, molecular liquids.

List of papers

This thesis consists of an introductory part and five research papers, which are referred to by the roman numerals **I** - **V** throughout the text.

I M. Hakala, **K. Nygård**, S. Manninen, L. G. M. Pettersson, and K. Hämäläinen, *Intra- and intermolecular effects in the Compton profile of water*, Physical Review B **73**, 035432 (2006).

II M. Hakala, **K. Nygård**, S. Manninen, S. Huotari, T. Buslaps, A. Nilsson, L. G. M. Pettersson, and K. Hämäläinen, *Correlation of hydrogen bond lengths and angles in liquid water based on Compton scattering*, The Journal of Chemical Physics **125**, 084504 (2006).

III **K. Nygård**, M. Hakala, S. Manninen, A. Andrejczuk, M. Itou, Y. Sakurai, L. G. M. Pettersson, and K. Hämäläinen, *Compton scattering study of water versus ice Ih: Intra- and intermolecular structure*, Physical Review E **74**, 031503 (2006).

IV **K. Nygård**, M. Hakala, T. Pylkkänen, S. Manninen, T. Buslaps, M. Itou, A. Andrejczuk, Y. Sakurai, M. Odelius, and K. Hämäläinen, *Isotope quantum effects in the electron momentum density of water*, The Journal of Chemical Physics (2007), accepted for publication.

V **K. Nygård**, M. Hakala, S. Manninen, K. Hämäläinen, M. Itou, A. Andrejczuk, and Y. Sakurai, *Ion hydration studied by x-ray Compton scattering*, Physical Review B **73**, 024208 (2006).

The author of this thesis is a contributing author of papers **I** - **II** and the principal author of papers **III** - **V**. He has planned and conducted the experiments and has been responsible for the data analysis. Moreover, he has performed part of the computations in the included papers: the three-dimensional water clusters of paper **I**, the direct comparison between normal and heavy water of paper **IV**, and the computations of paper **V**. Finally, he has had an active role in the interpretation of the results.

Contents

1 Introduction

Compton scattering is inelastic x-ray scattering at large energy and momentum transfers. It can be used to probe the ground state of the electron system. Its history dates back to the 1920s, when Compton [1] and Debye [2] explained their experimental observations in terms of photons, at the time being a controversial concept. A few years later DuMond determined the Compton-scattering lineshape of beryllium [3], thus providing the first indisputable experimental proof of the conduction electrons obeying the novel Fermi-Dirac statistics.

Despite the aforementioned impressive results, Compton scattering studies were scarce during the following decades. The resurrection of the technique is owing to the study of lithium by Cooper and coworkers [4] in the 1960s, combining x-ray tube sources and crystal analyzers. The subsequent introduction of solid-state detectors (SSDs) in the 1970s facilitated experimental work (see Ref. [5] for a review). During this latter period pioneering studies of water [6–9] and aqueous solutions [10, 11] were carried out, albeit experimental limitations hampered the extraction of detailed structural information.

A further advance was the advent of high-brilliance synchrotron-radiation sources, the immense increase in the incident x-ray flux making high-accuracy experiments feasible. While the pioneering experiments were carried out using SSDs [12, 13], the subsequent introduction of crystal spectrometers [14] eventually lead to the high momentum resolution currently obtainable [15]. Hence Compton scattering yields, e.g., detailed information about the Fermi surface [16, 17]. In recent years the technique has been applied to a variety of problems in the field of solid-state physics, including fermiology-related issues [18–20], high-pressure effects [21–24], and novel materials [25–29]. Notably, the so-called spin-polarized[1] Compton scattering, providing unique information about the ground-state spin density [30, 31], has benefited largely from the polarization properties of synchrotron radiation.

Subsequent to the discovery by Compton [1], the field of inelastic x-ray scattering expanded with the experimental observations of, e.g., non-resonant [32] and resonant [33] x-ray Raman scattering. Currently inelastic x-ray scattering is applied to studies of a variety of phenomena, such as various electronic excitations [34, 35] and phonons [36], Compton scattering being only a minor branch.

The inelastic x-ray scattering techniques have also been applied to studies of liquids [37], including work on the local structure [38] and dynamics [39] of water. Water exhibits numerous anomalous properties (see e.g. Ref. [40] for a review), which are predominantly traceable to its three-dimensional hydrogen-bond (H-bond) network [41]. Hence the local structure has attracted extensive interest since the 1930s. Nevertheless, no computational model currently exists that quantitatively conforms with all experimental observations [42]. This thesis describes a novel application of Compton scattering to structural studies of water, combining synchrotron-radiation-based experiments of unprecedented accuracy and

[1] Often referred to as 'magnetic Compton scattering'.

analysis within the density-functional theory (DFT). The technique is shown to provide unique information on the intra- and intermolecular structure, isotope quantum effects, and ion hydration.

Throughout this thesis, the system of atomic units (a.u.) is adopted for formulae and momenta ($\hbar = m = e = c\alpha = 1$ using standard notation), one atomic unit of momentum being $1.99 \cdot 10^{-24}$ kgms^{-1}. Lengths (distances) and energies are given in SI units and electron volts (eV), respectively.

2 Compton scattering

Compton scattering provides information about the electronic ground state of the target system [43, 44], the technique being particularly sensitive to the valence electrons (cf. the left panel of Fig. 1). Within the so-called impulse approximation, to be discussed in subsection 2.2, the double-differential scattering cross section can be expressed in terms of the so-called Compton profile, i.e. a one-dimensional projection of the ground-state electron momentum density. The electron momentum density is also accessible by the positron-annihilation [45], (γ,eγ) [46], and electron-momentum [47] spectroscopies. Upon comparison the versatility of Compton scattering should be noted, however, the technique being readily applicable to solids, liquids, and gases alike. Compton scattering is the only momentum-density probe hitherto applied to structural studies of liquid water.

Traditionally structural studies using x rays utilize diffraction, providing information on the electron charge density (cf. electron momentum density by Compton scattering). The reader is referred to Ref. [48] for a review on x-ray diffraction from water. Upon comparison a particular characteristic should be noted: contrariwise to x-ray diffraction, no formal connection between the Compton-scattering spectrum and the structure of the target system exists. This property is common to many spectroscopies [49–51]. Throughout this thesis the experimental data is interpreted in terms of structural effects by comparison with electronic-structure computations.

The well-known sensitivity of Compton scattering to chemical bonds is captured by the 'bond oscillation principle' [52]: the electron momentum density associated with a chemical bond exhibits damped oscillations in the bonding direction. The ensuing feature in the Compton profile of ice [53] (and water) has been interpreted as being predominantly induced by the nearest-neighbor exchange interaction [54–57]. The feature also includes smaller contributions from charge transfer and polarization [57, 58] as well as cooperative and anticooperative[2] many-body effects (see Ref. [56] and paper **I**). This partition is not unambiguous, however, as demonstrated by the debated interpretation in terms of covalency [53–56]. Nevertheless, the feature depends on the specific local structure [57]. Throughout this thesis it is thus used as an effective fingerprint of the intra- and intermolecular structure.

[2]Following Ref. [59], cooperative (anticooperative) effects refer to negative (positive) non-additive contributions to the total energy.

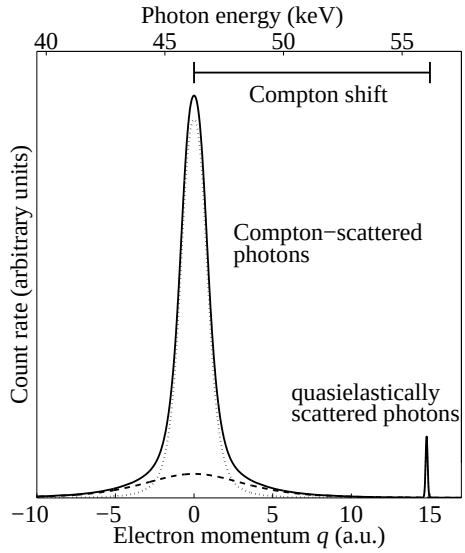

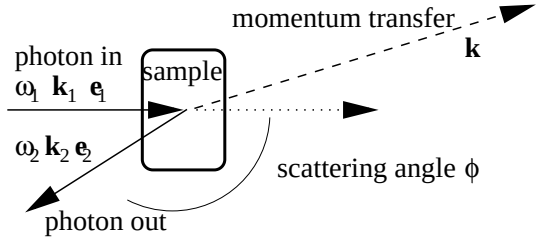

Fig. 1: Schematic representation of Compton scattering. **Left:** The scattering spectrum from water. The dashed and dotted lines correspond to scattering from the core (i.e. oxygen $1s$) and valence electrons, respectively. **Right:** The scattering process.

2.1 Non-resonant inelastic x-ray scattering

Throughout this thesis, Compton scattering refers to a process schematically presented in the right panel of Fig. 1. The incident (scattered) photon energy is denoted by ω_1 (ω_2), momentum by $\mathbf{k}_1$ ($\mathbf{k}_2$) and polarization by $\mathbf{e}_1$ ($\mathbf{e}_2$). The initial (final) state of the target is denoted by $|I\rangle$ ($|F\rangle$) and its energy by ϵ_I (ϵ_F). The energy and momentum transfers to the recoil electron are denoted by $\omega = \omega_1 - \omega_2$ and $\mathbf{k} = \mathbf{k}_1 - \mathbf{k}_2$, respectively.

In the non-relativistic, non-resonant limit the double-differential scattering cross section can be expressed as [60, 61]

$$\frac{d^2\sigma}{d\Omega d\omega_2} = \left(\frac{d\sigma}{d\Omega}\right)_{\mathrm{Th}} S\left(\mathbf{k},\omega\right), \tag{1}$$

where Ω denotes a solid angle. The Thomson cross section, representing the electron-photon coupling, is given by[3]

$$\left(\frac{d\sigma}{d\Omega}\right)_{\mathrm{Th}} = r_0^2 \left(\frac{\omega_2}{\omega_1}\right) \left(\mathbf{e}_1 \cdot \mathbf{e}_2\right)^2, \tag{2}$$

r_0 being the classical electron radius. The response of the electrons to the probe is included in the so-called dynamic structure factor, which is given by

$$S\left(\mathbf{k},\omega\right) = \sum_F \left| \langle F| \sum_j e^{i\mathbf{k}\cdot\mathbf{r}_j} |I\rangle \right|^2 \delta\left(\omega + \epsilon_I - \epsilon_F\right). \tag{3}$$

Here the summation is over the final states of the target system.

The dynamic structure factor carries information on the spatiotemporally correlated motion of the scattering particles. Following van Hove [63] it can be rewritten using a time

[3] A proper treatment of polarization would include the so-called Stokes parameters. In the present studies the effect of the synchrotron-radiation polarization properties is limited to the multiple-scattering contribution (see, e.g., Ref. [62]).

integral as

$$S\left(\mathbf{k},\omega\right)=\frac{1}{2\pi}\int_{-\infty}^{\infty}dt\ e^{i\omega t}\langle I|\sum_{i,j}e^{-i\mathbf{k}\cdot\mathbf{r}_i(0)}e^{i\mathbf{k}\cdot\mathbf{r}_j(t)}|I\rangle. \tag{4}$$

The strong dependence on the energy and momentum transfers should be noted, proper limits being (ξ_C and ω_C denote characteristic lengths and energies of the system, respectively):

- Small momentum transfer ($|\mathbf{k}|\xi_C \ll 1$): Collective behavior of the many-particle system is probed. The energy transfer ($\omega \sim \omega_C$) determines the type of collective excitations observed (such as phonons or plasmons).

- Large momentum transfer ($|\mathbf{k}|\xi_C \gg 1$): Single-particle excitations are probed. Throughout this thesis Compton scattering is defined in the large energy transfer limit ($\omega \gg \omega_C$), which constitutes the impulse approximation.

In the following subsection the latter limit is studied in more detail.

2.2 Impulse approximation

The present Compton-scattering data is interpreted within the impulse approximation. Following the formal justification provided by Eisenberger and Platzman [64], with Eq. (3) for simplicity rewritten in the single-particle picture, the dynamic structure factor is given by

$$S\left(\mathbf{k},\omega\right)\simeq\frac{1}{2\pi}\int_{-\infty}^{\infty}dt\ e^{i\omega t}\sum_{i}^{\text{occ}}\sum_{f}^{\text{unocc}}\langle i|e^{-i\mathbf{k}\cdot\mathbf{r}}|f\rangle\langle f|e^{i(H_0+V)t}\ e^{i\mathbf{k}\cdot\mathbf{r}}\ e^{-i(H_0+V)t}|i\rangle. \tag{5}$$

Here H_0 and V denote the free-electron Hamiltonian and the potential, respectively, and the sum is over the occupied (unoccupied) single-particle initial (final) states $|i\rangle$ ($|f\rangle$) with energy ϵ_i (ϵ_f). The essence of the impulse approximation can be stated as follows: For large energy transfers ($\omega \gg \langle[H_0,V]\rangle^{1/2}$) only a short interval of time ($t \lesssim \omega^{-1}$) contributes to the above time integral, justifying the approximation

$$e^{i(H_0+V)t}=e^{iH_0t}e^{iVt}e^{-[H_0,V]t^2/2}\ldots\simeq e^{iH_0t}e^{iVt}. \tag{6}$$

Since V and $\mathbf{r}$ commute, Eq. (5) can further be simplified as

$$S^{\text{IA}}\left(\mathbf{k},\omega\right)\simeq\frac{1}{2\pi}\int_{-\infty}^{\infty}dt\ e^{i\omega t}\sum_{i}^{\text{occ}}\sum_{f}^{\text{unocc}}\langle i|e^{-i\mathbf{k}\cdot\mathbf{r}}|f\rangle\langle f|e^{iH_0t}\ e^{i\mathbf{k}\cdot\mathbf{r}}\ e^{-iH_0t}|i\rangle. \tag{7}$$

Due to the instantaneous nature of the scattering process, the target has no time to relax; thus the potential cancels between initial and final states. Consequently the scattered photons carry no information about the latter states.

Assuming the recoil electron to be free in its final state, the last expression can be rewritten as[4]

$$S^{\mathrm{IA}}(\mathbf{k},\omega) \simeq \sum_{i}^{\mathrm{occ}} \int d\mathbf{p}\, |\chi_i(\mathbf{p})|^2\, \delta\left(\omega - |\mathbf{k}|^2/2 - \mathbf{k}\cdot\mathbf{p}\right). \tag{8}$$

Here $\chi_i(\mathbf{p})$ denotes the momentum-space wave function representing the single-particle state $|i\rangle$. Inserting the ground-state electron momentum density $N(\mathbf{p}) = \sum_i^{\mathrm{occ}} |\chi_i(\mathbf{p})|^2$ and assuming an isotropic target (e.g. a liquid), Eq. (8) leads to

$$S^{\mathrm{IA}}(\mathbf{k},\omega) \simeq \frac{1}{|\mathbf{k}|} J(q), \tag{9}$$

where the isotropic Compton profile is defined as

$$J(q) = \frac{1}{2}\int_0^{4\pi} d\Omega \int_{|q|}^{\infty} dp\, p\, N(\mathbf{p}). \tag{10}$$

The scalar momentum variable $q = (\omega - |\mathbf{k}|^2/2)/|\mathbf{k}|$ is the projection of the electron momentum $\mathbf{p}$ along the scattering vector $\mathbf{k}$. Due to the incoherent nature of the scattering process, individual electrons provide additive contributions to the Compton profile (cf. the left panel of Fig. 1). It should be noted that the main results outlined here persist upon using more sophisticated methods, e.g., including relativistic [65, 66] or final-state effects [67–69]. The deviations from the impulse approximation have been studied extensively [70–73].

The connection between the scalar momentum variable q and the experimental parameters, i.e. the incident (scattered) photon energy ω_1 (ω_2) and the scattering angle ϕ, is given by relativistic kinematics [65, 66]. To a good approximation

$$q \simeq \frac{|\mathbf{k}|}{2} - \frac{(\omega_1 - \omega_2)}{c}\sqrt{\frac{1}{4} + \frac{c^4}{2\omega_1\omega_2(1-\cos\phi)}}. \tag{11}$$

Throughout this thesis the high-energy side of the intrinsically symmetric Compton profile corresponds to positive momentum values (cf. the left panel of Fig. 1).

2.3 Computations

In this thesis the experimental data is interpreted using model computations. In these computations the electron momentum density, and the ensuing Compton profile, is determined within the DFT. Next the computations are briefly reviewed.

Density-functional theory

Within the so-called Kohn-Sham DFT [74, 75], the many-body ground state of a system of interacting electrons is represented in terms of fictitious, non-interacting single-particle

[4] The terms $|\mathbf{k}|^2/2$ and $\mathbf{k}\cdot\mathbf{p}$ govern the energy position (i.e. the so-called Compton shift) and the width of the Compton scattering spectrum, respectively (cf. the left panel of Fig. 1).

states [76, 77]. Accordingly, the correct ground-state energy can, in principle, be found by varying the total energy functional $E[n]$ [74] [$n(\mathbf{r})$ or n denoting the electron density]. Assuming a system of electrons in an external potential due to a set of nuclei, the total energy functional is formally expressed as

$$E[n] = T[n] + \frac{1}{2}\int d\mathbf{r}\int d\mathbf{r}'\frac{n(\mathbf{r})n(\mathbf{r}')}{|\mathbf{r}-\mathbf{r}'|} - \sum_l \int d\mathbf{r}\frac{Z_l n(\mathbf{r})}{|\mathbf{R}_l - \mathbf{r}|} + E_{\mathrm{nuc}}(\{\mathbf{R}_l\}) + E_{\mathrm{xc}}[n]. \quad (12)$$

Here $\{\mathbf{R}_l\}$ describes the nuclei positions and $\{Z_l\}$ the corresponding atomic numbers. $T[n]$ denotes the kinetic energy of the fictitious non-interacting electrons, while the second, third, and fourth terms on the right-hand side correspond to the electron-electron, electron-nucleus, and nucleus-nucleus Coulomb interactions, respectively. The last term, the so-called exchange-correlation functional $E_{\mathrm{xc}}[n]$, is composed of the energy terms neglected hitherto. This approach would be exact, if the exchange-correlation functional was known correctly. However, generally one resorts to approximate functionals.

For practical computations a system of non-interacting electrons moving in a common potential is constructed [75]. The electron density, equaling to that of the true interacting system, is specified in terms of orthogonal single-particle wave functions as

$$n(\mathbf{r}) = \sum_i \left|\psi_i^{\mathrm{KS}}(\mathbf{r})\right|^2. \quad (13)$$

Here $\psi_i^{\mathrm{KS}}(\mathbf{r})$ denotes a so-called Kohn-Sham orbital and the sum is over the occupied states. The variation of Eq. (12) thus leads to the self-consistent Kohn-Sham equations

$$\left[-\frac{1}{2}\nabla^2 + V_{\mathrm{KS}}(\mathbf{r})\right]\psi_i^{\mathrm{KS}}(\mathbf{r}) = \epsilon_i \psi_i^{\mathrm{KS}}(\mathbf{r}), \quad (14)$$

where ϵ_i is the eigenvalue corresponding to the orbital $\psi_i^{\mathrm{KS}}(\mathbf{r})$ and the potential is given by

$$V_{\mathrm{KS}}(\mathbf{r}) = \int d\mathbf{r}'\frac{n(\mathbf{r})}{|\mathbf{r}-\mathbf{r}'|} - \sum_l \frac{Z_l}{|\mathbf{R}_l - \mathbf{r}|} + \frac{\delta E_{\mathrm{xc}}[n]}{\delta n(\mathbf{r})}. \quad (15)$$

The many-body system of interacting electrons can thus be treated, in principle exactly, as a system of non-interacting particles, the interactions between the electrons being included implicitly in the potential. The only physically relevant quantities within this approach, however, are the electron density and the total energy.

In the present work, the momentum density is computed by Fourier transforming the individual Kohn-Sham orbitals of the determinant wave function separately [78],

$$N(\mathbf{p}) = \sum_i (2\pi)^{-3}\left|\int d\mathbf{r} \mathrm{e}^{-i\mathbf{p}\cdot\mathbf{r}}\psi_i^{\mathrm{KS}}(\mathbf{r})\right|^2. \quad (16)$$

The Kohn-Sham orbitals are formally merely auxiliary functions; nevertheless, they can carry valuable information about the electron system [79]. The approximation of using

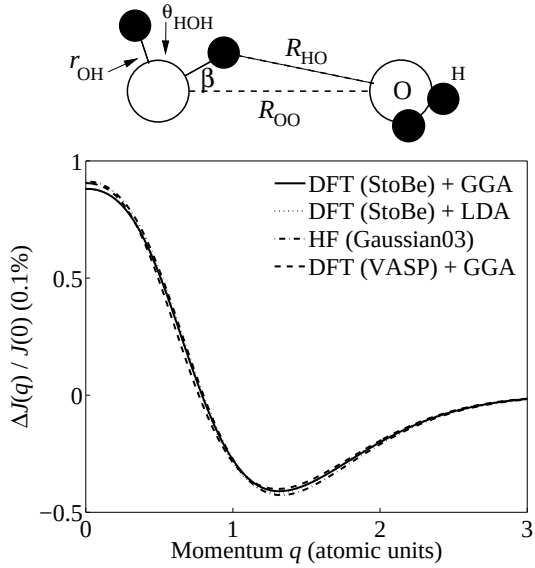

Fig. 2: **Top:** Geometric definitions for a water dimer. **Bottom:** Influence of various computational approximations on the difference between Compton profiles of water monomers. The monomers are defined by the intramolecular bond lengths $r_{\mathrm{OH}} = 0.972$ Å and $r_{\mathrm{OH}}^{\mathrm{ref}} = 0.968$ Å, respectively.

them as the single-particle wave functions in computing the Compton profile of water has been shown reasonable by comparison with Hartree-Fock (HF) and Møller-Plesset second-order perturbation theory calculations [54, 57]. However, a verification of the adopted approach by comparison to more sophisticated computations, e.g. coupled-cluster calculations [80], would be highly useful.

Computational approximations

Throughout this thesis, the experimental data was interpreted using atomic-cluster-based model computations. Specifically, in papers **II**-**IV** temperature-dependent H-bond length and angle distributions for water [50] and an *ad hoc* computational method (outlined in paper **I**) based on additive nearest-neighbor interactions only was used. Within this approach, which is in line with previous studies of water [9] and hydrocarbons [81], the nearest-neighbor contributions are treated as mutually independent perturbations to the monomer Compton profile, neglecting many-body effects. Such an approach was preferred over *ab initio* simulations in order to obtain specific information on the various structural parameters observed in the Compton profile. Nonetheless, the complex local structure of water and particularly aqueous solutions, not easily accessible by model calculations, necessitates also comparison with more sophisticated computational approaches. Hence computations based on *ab initio* Car-Parrinello molecular-dynamics (MD) [82] configurations were also included in paper **IV**. However, the lack of quantitative agreement with experimental Compton-scattering data could imply a necessity of including nuclear quantum effects in the Car-Parrinello MD approach [83].

The influence of various computational approximations on the difference of Compton profiles is demonstrated for water monomers in the bottom panel of Fig. 2. The monomer and reference monomer are specified by the intramolecular bond lengths $r_{\mathrm{OH}} = 0.972$ Å and $r_{\mathrm{OH}}^{\mathrm{ref}} = 0.968$ Å, respectively (see the top panel of Fig. 2 for the geometric definitions). The

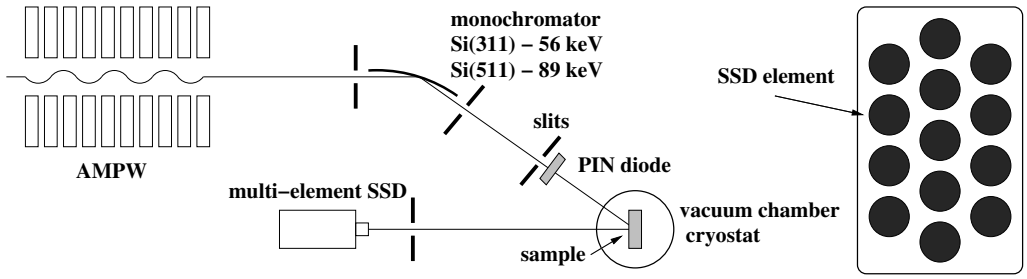

Fig. 3: **Left:** Schematic presentation of beamline ID15B. **Right:** Schematic picture of the multi-element SSD.

difference of Compton profiles computed using an extension [57] of the StoBe-deMon code [84] within the generalized-gradient approximation [85, 86] (GGA) of the DFT is shown. Linear combinations of contracted Gaussian basis functions are utilized for the Kohn-Sham orbitals. For the oxygen atoms a TZVP-type basis set is used, whereas a primitive set augmented by one p-function in a [3s,1p] contraction is employed for the hydrogen atoms. The corresponding computation within the local-density approximation [87, 88] (LDA) is also presented, indicating the effect of the functionals. Next, the effect of the level of theory is demonstrated by comparison with HF-based computations using the Gaussian03 code [89], utilizing a TZVP-type basis set. Finally, the effect of the basis set is studied by comparison with gradient-corrected [90, 91] computations within the DFT using an extension [92] of the plane-wave-based VASP code [93, 94]. The minor influence of the computational approximations when considering differences between Compton profiles of water monomers (and dimers) should be noted.

3 Experiments

The experimental work described in this thesis was carried out at the beamlines ID15B of the European Synchrotron Radiation Facility (ESRF, Grenoble, France) and BL08W of the Super Photon Ring - 8 GeV (SPring-8, Hyogo, Japan). Both beamlines are designed for Compton-scattering studies using monochromatic incident x rays, with the radiation source in both cases being a wiggler. At beamline ID15B [95] the x-ray energy was either $\omega_1 \simeq$ 56 keV or $\omega_1 \simeq 89$ keV, whereas at station A (B) of beamline BL08W [96] harder incident x rays with $\omega_1 \simeq 176$ keV ($\omega_1 \simeq 115$ keV) were used. The maximum incident x-ray flux at the sample is comparable at ID15B and BL08W [approximately 10^{12} photons/s/(maximum beam size)]. In the following the beamlines and the experimental details will be reviewed.

3.1 Beamline ID15B (ESRF)

At beamline ID15B, schematically presented in Fig. 3, the incident x rays are produced by a seven-period asymmetric multipole permanent-magnet wiggler (AMPW). In the present studies (papers **II** and **IV**) horizontally focusing Johann-type Si(311) and Laue-type Si(511)

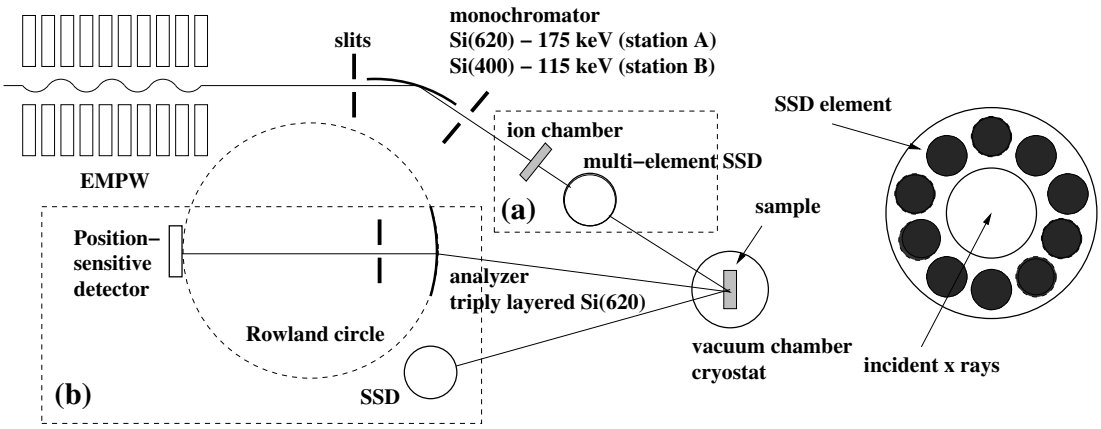

Fig. 4: **Left:** Schematic presentation of beamline BL08W: (a) the multi-element SSD and (b) the Cauchois-type spectrometer setup. **Right:** Schematic picture of the multi-element SSD.

monochromators were used, yielding incident x rays with $\omega_1 \simeq 56$ keV and $\omega_1 \simeq 89$ keV energy, respectively. The incident x-ray flux was monitored using a Si PIN diode, working in photovoltaic mode.

The high-resolution scanning crystal spectrometers installed at ID15B yield momentum resolutions (i.e. the full-width-at-half-maximum of the resolution functions) below 0.1 a.u. [95, 97, 98]. However, since the interaction between the water molecules is expected to induce only a weak feature in the Compton profile [57], the limited statistical accuracy hampers structural studies of water and aqueous solutions. Hence a 13-element Ge SSD was employed, providing spectra with only moderate momentum resolution but superior statistical accuracy. Such a detection system has previously been applied, e.g., to spin-polarized Compton scattering studies [99]. The use of a multi-element SSD, each element utilizing individual electronics, is crucial to achieve the accuracy necessary for the present studies.

With such an experimental setup, the moderate momentum resolution Δq depends predominantly on the energy resolution of the SSD (typically $\Delta\omega_2 \gtrsim 400$ eV and $\Delta q \simeq 0.6$ a.u. in the present studies). However, the use of the multi-element SSD leads to the aforementioned extremely small statistical inaccuracy of the Compton profile difference [typically below 0.02% of $J(0)$ at the Compton peak (i.e. at $q = 0$ a.u.)]. The experimental parameters are summarized in Table 1.

3.2 Beamline BL08W (SPring-8)

At beamline BL08W, schematically presented in Fig. 4, the incident radiation is produced by a 37-period elliptical multipole wiggler (EMPW) [100]. An asymmetric Johann-type Si(620) [a doubly bent Si(400)] monochromator was used at station A (B), providing $\omega_1 \simeq 176$ keV ($\omega_1 \simeq 115$ keV) incident x rays. Two different experimental setups were used, utilizing either a ten-element Ge SSD or a Cauchois-type spectrometer, the incident x-ray

Paper	Beamline	ϕ (°)	ω_1 (keV)	Δq (a.u.)	σ (0.1%)	Beam size (mm^2)
II	ID15B	160	56	0.64	0.20	0.3(H)×1.0(V)
III	BL08W(B)	178	115	0.63	0.16	2.0(H)×2.0(V)
IV	ID15B	165	89	0.54	0.16	0.2(H)×0.5(V)
IV	BL08W(A)	172	176	0.45	0.18	1.2(H)×0.6(V)
V	BL08W(B)	165	115	0.20	1.3	1.0(H)×2.0(V)

Table 1: Experimental parameters. The inaccuracy σ of the difference between Compton profiles at the Compton peak is given as fraction of $J(0)$. The horizontal (H) and vertical (V) beam sizes are given at the sample.

flux being monitored using an ionization chamber (Ge SSD) in the former (latter) case.

In papers **III** and **IV** a similar detection system as described above was used. At BL08W, however, the multi-element Ge SSD was 'doughnut'-shaped (see the right panel of Fig. 4): the ten elements were positioned symmetrically on the arc of a circle, while the incident x rays passed through the center. It should be noted that this choice of scattering geometry hampers the reduction of background by shielding. The momentum resolutions achieved at BL08W and ID15B are comparable, whereas an improved statistical accuracy is obtained at the former beamline.

In paper **V** the detection system consisted of the standard Cauchois-type high-resolution spectrometer [101, 102], utilizing a triply layered Si(620) bent-crystal analyzer (radius of curvature $R = 3650$ mm). The photons were detected using a position-sensitive detector, which utilizes an x-ray image intensifier and a digital CCD camera. The middle analyzer crystal and the detector share the same Rowland circle ($R = 1825$ mm). The momentum resolution $\Delta q \simeq 0.20$ a.u. was significantly improved compared with a multi-element SSD, whereas the statistical accuracy was limited.

Upon comparing the beamlines BL08W and ID15B a particular characteristic should be mentioned. SPring-8 is operated in the so-called top-up mode [103] (i.e. with quasi-continuous filling of electrons), the temporal variation of the stored electron-beam current being below 0.1% (cf. approximately 15% variation of the current in twelve-hour cycles at the ESRF). Consequently the thermal stability of the x-ray optics and the count-rate dependent operation of the multi-element SSD are greatly enhanced. Thus data of improved quality is obtainable at BL08W, facilitating studies of the subtle H-bond effects in the Compton profile of water.

3.3 Experimental details

The experimental work constitutes a major part of this thesis. In the following details about the data analysis and sample environment will be reviewed.

Data analysis

There are several important corrections that need to be applied to the collected data in order to extract the Compton profile. The data was corrected for absorption and background, the latter determined by measuring scattering from the empty cell, before applying a relativistic conversion of the double-differential cross section (as function of the scattered photon energy ω_2) to the Compton profile (in terms of the momentum variable q) [66]. The contribution of multiple scattering was studied both computationally [62, 104, 105] (papers **II-V**) and experimentally (paper **V**). When using the Cauchois-type spectrometer (paper **V**) the efficiency of the detection system, i.e. the reflectivities of the analyzer crystals and the efficiency of the position-sensitive detector, was determined utilizing x-ray fluorescence emission of thallium and bismuth. The energy resolutions were determined utilizing characteristic γ- and x-ray spectra. Finally the positive and negative momentum sides of the (in principle) intrinsically symmetric Compton profiles were averaged (papers **II-IV**).

The temporally varying incident x-ray flux at synchrotron-radiation laboratories necessitates continuous monitoring, albeit the top-up mode (partly) eliminates this requirement [103]. However, since the Compton-scattering spectra in the present studies were collected using energy-dispersive methods, as compared to using a scanning spectrometer [73], the normalization with incident x-ray flux is less significant. The same holds for the closely related dead-time correction, which is due to a too narrow dynamic range of the detection system. Nevertheless, for proper background subtraction these issues are of importance.

Since the changes in the Compton profiles studied in the present work are very small [typically about 0.1% of $J(0)$ at the Compton peak], the consistency of the data is crucial. Thus it was monitored carefully throughout the experiments. In practice, spectra were saved every 10 (30) minutes in papers **II-IV** (**V**) and verified to be consistent before added. Due to experimental instabilities individual spectra were further shifted (typically within 0.01 a.u. of momentum).

Sample environment

Two different types of sample confinement were used in the present studies. In papers **II-III** and **V** metal cells with 25 μm thick polyimide (i.e. Kapton) windows were used. The 2 mm thick (10 mm in paper **V**) sample cells were cylindrically symmetric with respect to the incident x-ray path. In paper **IV** thin-walled (10 μm thick) borosilicate glass capillaries with a 2 mm diameter were used. Two particular characteristics of the sample cells should be noted. First, the minor diffusion of water through the polyimide windows poses a problem at elevated temperatures. Second, the sample thickness is well defined only when using the glass capillaries. In particular, the minimization of volume-dependent effects by using the same capillary is crucial when comparing Compton profiles acquired from different liquids.

Throughout this thesis the samples were inserted in vacuum chambers, thus minimizing

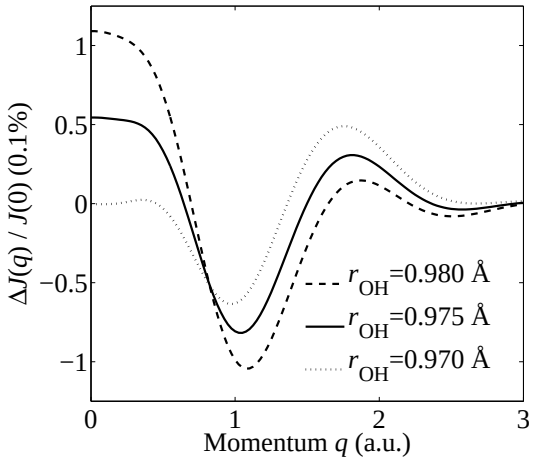

Fig. 5: Impact of r_{OH} on the difference between computational Compton profiles of water dimers. The dimer is defined by $R_{\mathrm{HO}} = 1.90$ Å and $\beta = 0°$ (with variable r_{OH}), while the reference dimer is specified by $R_{\mathrm{HO}}^{\mathrm{ref}} = 1.783$ Å, $r_{\mathrm{OH}}^{\mathrm{ref}} = 0.98$ Å, and $\beta^{\mathrm{ref}} = 0°$. The solid line equals, within the present experimental accuracy, the average of the dashed and dotted lines.

the background due to scattering from air. However, the direct comparison between normal and heavy (i.e. deuterated) water Compton profiles (paper **IV**), utilizing the same unsealed glass capillary for confining both samples, was carried out in helium atmosphere. The temperature of the sample was controlled within 0.1 K using either standard cryostats (papers **II-III**) or a Peltier-based system (paper **IV**).

4 Local structure of water

This thesis comprises a novel application of Compton scattering to structural studies of molecular liquids,[5] enabled by third-generation synchrotron-radiation sources. Notably, the systematic studies included focus on water, providing unique intra- and intermolecular structural information. In the following subsections the local structure of water, as obtained by other techniques, and the results of the present work will be briefly reviewed.

4.1 Intra- and intermolecular structure

The V-shaped water molecule, consisting of 2 hydrogen atoms covalently bonded to an oxygen atom, has the average intramolecular bond length $r_{\mathrm{OH}} \sim 0.97$ Å and angle $\theta_{\mathrm{HOH}} \sim 106°$ in the liquid state [107]. The interaction between the molecules is governed by the H bond. Following Ref. [108] the O-H$\cdots$O' interaction in water is defined a H bond, if it (i) is local and (ii) O-H acts as a proton donor to the acceptor O' (H, O, and O' denoting a hydrogen and two adjacent oxygen atoms, respectively). In practice, one often resorts to various energetic or geometric definitions. The complex nature of the H bond in water, exhibiting, e.g., cooperativity [59] and the disputed charge-transfer effects [109–111], should also be noted.

[5]Throughout this thesis the term 'molecular liquid' denotes a liquid with strong primary (i.e. intramolecular) and moderate or weak secondary (i.e. intermolecular) interatomic bonding. The reader is referred to Ref. [106] for a review on liquids.

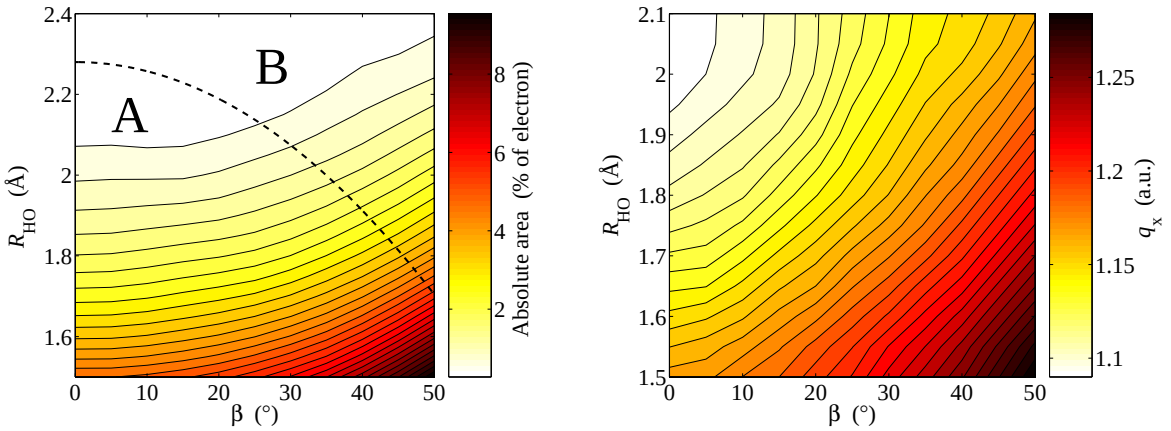

Fig. 6: Sensitivity of the difference between Compton profiles to radial (R_{HO}) and angular (β) distortions in the H-bond geometry of a water dimer. The reference consists of two isolated water monomers. **Left:** Absolute area of the difference between Compton profiles. The dashed line defines a geometrical criterion for intact (A) and weakened/broken (B) H bonds [51]. **Right:** Momentum position of the extremum at $q_x \sim 1$ a.u. in the difference between Compton profiles (cf. Fig. 5).

The water molecules form three-dimensional H-bond networks upon condensation [41]. Upon freezing at ambient pressure hexagonal ice Ih is formed (the reader is referred to Ref. [112] for a review on ice). In ice Ih, the oxygen atoms are interconnected by nearly linear H bonds in a tetrahedral nearest-neighbor arrangement ($R_{\mathrm{OO}} \sim 2.75$ Å). In accordance with the so-called 'ice rules', one hydrogen atom is positioned between each adjacent oxygen-oxygen pair. Consequently each molecule participates in four H bonds, i.e. both donating and accepting two protons.

In contrast, liquid water is a dynamical system with the individual H bonds continually breaking and reforming [41]. Traditionally its average structure has been studied using x-ray [48] and neutron diffraction [113] as well as classical [42] and *ab initio* [114] MD simulations. Accordingly, the prevailing picture of a quasitetrahedral local structure has emerged: the average water molecule participates in nearly four H bonds with its nearest neighbors, the H bonds in water being radially and angularly distorted compared to those in ice Ih. This picture was recently contested [51], however, x-ray spectroscopic data being interpreted as reflecting a predominance of asymmetric bonding in water, with the majority of molecules participating only in two intact H bonds. This latter interpretation is under active debate [115–122].

Intra- and intermolecular effects

The distinct fingerprints in the Compton profile of water induced by various intra- and intermolecular structural parameters were studied systematically in paper **I**. In line with the 'bond oscillation principle' [52], the intermolecular fingerprints oscillate more rapidly as compared with the intramolecular ones (see Ref. [57] and paper **I**). A variation of the

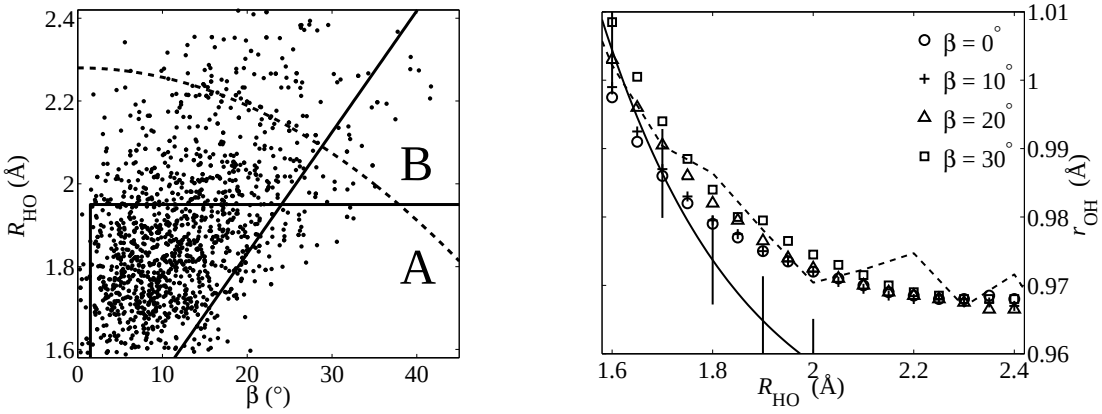

Fig. 7: Structural correlations in water based on Compton scattering. **Left:** Intermolecular correlation between the length and angular distortions of the H bond. The solid lines delineate different excluded regions for the H-bond geometries studied in paper **II**, while the dots represent H-bond geometries derived from Car-Parrinello MD simulations [123]. The dashed line defines the geometrical H-bond criterion [51] depicted in the left panel of Fig. 6. **Right:** Correlation between the intramolecular bond length and the corresponding H-bond geometry. The solid (dashed) line is derived from crystal hydrates [124] (Car-Parrinello MD simulations [123]).

intramolecular structural parameters, i.e. the intramolecular bond length r_{OH} and angle θ_{HOH}, induce mutually distinct fingerprints in the Compton profile. The influence of the intramolecular oscillations should also be noted. The effect of including small O-H stretch and H-O-H bend vibrations in the computational Compton profile, as compared to using the first moment of the corresponding distributions, was found to be negligible compared to the present experimental accuracy (cf. Fig. 5).

The sensitivity of Compton scattering to radial and angular distortions in the H-bond geometry of a water dimer was also studied extensively in paper **II**. The absolute area of the difference between Compton profiles was found to predominantly reflect radial distortions (see the left panel of Fig. 6). Contrariwise to the aforementioned intramolecular bond elongations, radial distortions of the H-bond geometry induce a fingerprint in the Compton profile which exhibits a notable nonlinearity in terms of the absolute area. The difference between Compton profiles was also found to reflect angular distortions of the H bond (see the right panel of Fig. 6), albeit these are not as strongly manifested as the radial distortions. Thus Compton scattering is found to primarily probe the H-bond length distribution (adopting a typical geometric H-bond criterion [51] as depicted in the left panel of Fig. 6).

Structural correlations

The present Compton-scattering studies (papers **II** and **III**) provide structural information on water primarily in terms of structural correlations. In paper **II** the intermolecular corre-

lation between the length and angular distortion of the H bond was studied. By comparing model computations with experimental data, a necessity of excluding short and largely bent H-bond geometries was demonstrated for liquid water. A similar result was also obtained in paper **III** from the comparison between the Compton profiles of water and polycrystalline ice Ih. The finding is in qualitative agreement with average results for crystal hydrates [125] and H-bond geometries derived from Car-Parrinello MD simulations [123]. However, the detailed intermolecular correlation cannot be uniquely determined by Compton scattering. This is exemplified by the mutually distinct excluded regions for the H-bond geometries depicted in the left panel of Fig. 7, which could not be distinguished by Compton scattering. These results are valid also upon including a correlation between the intra- and intermolecular geometries (to be discussed in the following paragraph).

The average intramolecular bond length depends on the specific H-bond geometry, the former ranging from $r_{\mathrm{OH}} \simeq 0.98$ Å in ice Ih [112] to $r_{\mathrm{OH}} \simeq 0.958$ Å for isolated water monomers [126]. In paper **III** the detailed correlation between the intramolecular bond length and the corresponding H-bond geometry, i.e. $r_{\mathrm{OH}} = r_{\mathrm{OH}}(R_{\mathrm{HO}}, \beta)$, was studied. By comparing model computations with the experimental difference between water and polycrystalline ice Ih Compton profiles, a necessity of including such a correlation (presented in the right panel of Fig. 7) was demonstrated for liquid water. The found correlation is in good agreement with average results derived from crystal hydrates [124] and Car-Parrinello MD simulations [123]. In paper **IV** it was further successfully applied to the analysis of temperature-dependent water data.

Finally, the debated interpretation of x-ray spectroscopic data in terms of predominantly asymmetric bonding in water [51] should be commented. The Compton profile of water was not found to be sensitive to whether the bonding of individual molecules is symmetric or asymmetric; thus the present studies can neither corroborate nor refute the claim of Ref. [51] regarding asymmetry. Based on computational analysis, the traditional picture of liquid water, in which the average number of intact H bonds per molecule is $n_{\mathrm{HB}} \simeq 3.5$ at room temperature, is consistent with the experimental data of the present studies. In principle the lowest limit obtainable in paper **III** was $n_{\mathrm{HB}} \geq 2.7$, adopting the geometrical H-bond criterion of Ref. [51].

4.2 Isotope quantum effects

Deuteration affects many properties of water: the dynamic behavior, the thermodynamic properties, and the local structure (see, e.g., Ref. [40]). These effects, collectively referred to as isotope quantum effects, have partly been attributed to a larger zero-point energy of normal compared to heavy water [83]. Experimentally the structural isotope effects have been studied primarily by high-energy x-ray diffraction [127, 128]. Accordingly, isotopic substitution affects the structural disorder, the local intermolecular structure of heavy water at room temperature approximately corresponding to that of normal water at a lower temperature ($\Delta T \sim 6$ °C). This effective temperature offset has been found to decrease with

temperature [129]. However, simulations reproduce only qualitatively the experimentally observed difference between the structure factors [83, 130]. Hence complementary information on the structural isotope quantum effects could shed some light on this important issue.

Paper **IV** presents a Compton-scattering study addressing the isotope quantum effects in water. By comparison with model computations, the difference between experimental room-temperature Compton profiles of normal and heavy water is attributed predominantly to intramolecular structural differences. The major contribution is found to be induced by a difference in the intramolecular bond lengths, i.e. $\Delta r = r_{\mathrm{OH}} - r_{\mathrm{OD}} \approx 0.004$ Å (cf. the bottom panel of Fig. 2). The interpretation in terms of intramolecular structural differences is in good agreement with previous reports (see, e.g., Ref. [127]). Furthermore, the temperature-induced changes in the Compton profile are distinctly different for normal and heavy water. This is again interpreted as primarily reflecting intramolecular structural differences. It should be noted that the mere observation of isotope effects in the Compton profile of water owes to the very good accuracy and consistency of the experimental data. It is also noteworthy that no temperature dependence of the intramolecular structure of water has been observed by x-ray diffraction [127, 131], since it is primarily sensitive to the intermolecular structure. Given this predominant sensitivity of Compton scattering to the intramolecular structure, the technique thus provides unique structural information on the subtle isotope quantum effects in water.

4.3 Ion hydration

Water is a strong polar solvent, which can completely dissolve strong ionic salts such as lithium chloride. The hydration of charged ions can predominantly be attributed to the ion-dipole interaction, the water molecules in the first hydration shell orienting their dipoles with respect to the charged ion. However, e.g. charge-transfer effects might also be of importance [132]. Moreover, the effect of ion hydration on the structure of water has generally been assumed significant, some ions strengthening and some weakening the H-bond network (i.e. the so-called 'structure makers' and 'structure breakers', respectively). A recent study contested this latter picture, however, with no structural changes in the H-bond network beyond the first hydration shell being observed upon ion hydration [133].

The traditional experimental techniques for structural studies of aqueous solutions are x-ray and neutron diffraction (see Ref. [134] for a seminal paper on aqueous LiCl). However, since aqueous LiCl is composed of four elements, it is characterized by a total of ten partial radial distribution functions, which hampers experimental interpretation. Consequently there is a large variation in the experimental results [135, 136]. Similarly classical MD simulations suffer from severe limitations; in particular, the results depend strongly on the empirical force fields used in the simulations [137]. Hence complementary structural information on ion hydration would be highly important.

Pioneering Compton scattering studies of aqueous LiCl have previously been reported [10,

11], albeit proper structural information was not obtained due to experimental limitations. Paper **V** presents Compton-scattering experiments with significantly improved accuracy, thus demonstrating the feasibility of the technique for structural studies of ion hydration. By comparison with model computations, the experimental findings are interpreted as predominantly providing structural information on the first hydration shell. In particular, the study yields upper limits for the average nearest-neighbor oxygen-ion distances: $R_{\mathrm{OLi}} \lesssim 2.10$ Å and $R_{\mathrm{OCl}} \lesssim 3.15$ Å for lithium and chloride ions, respectively.

5 Concluding remarks

This thesis describes a series of systematic Compton-scattering experiments of unprecedented accuracy on various molecular liquids: water, heavy water, and aqueous lithium chloride. By comparison with model computations, the fingerprints in the Compton profile related to various structural parameters can be distinguished. Consequently the subtle changes in the Compton profile, induced e.g. by temperature, can be attributed to distinct intra- and intermolecular structural changes.

Throughout this thesis, the experimental data is interpreted using model computations, providing guidelines for future computational analysis. However, the complex local structure of water, and particularly aqueous solutions, is not quantitatively described by such simple computations. A challenging, but necessary, development of the computational analysis will thus be the inclusion of *ab initio* MD configurations, possibly also comprising nuclear quantum effects.

The present work demonstrates the feasibility of the Compton-scattering technique for structural studies of molecular liquids. Given its sensitivity to both intra- and intermolecular structural changes, it has been shown to provide unique information on these subtle effects. A continuation of the present work towards structurally more complex molecular liquids, such as simple alcohols and their aqueous solutions, is currently being planned.

References

[1] A. H. Compton, Phys. Rev. **21**, 483 (1923).

[2] P. Debye, Phys. Zeit. **24**, 161 (1923).

[3] J. W. M. DuMond, Phys. Rev. **33**, 643 (1929).

[4] M. Cooper, J. A. Leake, and R. J. Weiss, Philos. Mag. **12**, 797 (1965).

[5] B. Williams (ed.), *Compton Scattering* (McGraw-Hill, London, 1977).

[6] M. H. Whangbo, V. H. Smith Jr., E. Clementi, G. H. Diercksen, and W. von Niessen, J. Phys. B: Atom. Molec. Phys. **7**, L427 (1974).

[7] B. Williams, Acta Cryst. **A32**, 513 (1976).

[8] S. Manninen, T. Paakkari, and V. Halonen, Chem. Phys. Lett. **46**, 62 (1977).

[9] A. Seth and E. J. Baerends, Chem. Phys. Lett. **52**, 248 (1977).

[10] T. Paakkari, Chem. Phys. Lett. **55**, 160 (1978).

[11] A. Seth and E. J. Baerends, Chem. Phys. Lett. **64**, 165 (1979).

[12] M. Cooper, R. Holt, P. Pattison, and K. R. Lea, Commun. Phys. **1**, 159 (1976).

[13] R. S. Holt, M. Cooper, and K. R. Lea, J. Phys. E **11**, 68 (1978).

[14] G. Loupias, J. Petiau, A. Issolah, and M. Schneider, Phys. Stat. Sol. B **102**, 79 (1980).

[15] K. Hämäläinen, S. Manninen, C.-C. Kao, W. Caliebe, J. B. Hastings, A. Bansil, S. Kaprzyk, and P. M. Platzman, Phys. Rev. B **54**, 5453 (1996).

[16] Y. Sakurai, Y. Tanaka, A. Bansil, S. Kaprzyk, A. T. Stewart, Y. Nagashima, T. Hyodo, S. Nanao, H. Kawata, and N. Shiotani, Phys. Rev. Lett. **74**, 2252 (1995).

[17] C. Blaas, J. Redinger, S. Manninen, V. Honkimäki, K. Hämäläinen, and P. Suortti, Phys. Rev. Lett. **75**, 1984 (1995).

[18] S. Huotari, K. Hämäläinen, S. Manninen, S. Kaprzyk, A. Bansil, W. Caliebe, T. Buslaps, V. Honkimäki, and P. Suortti, Phys. Rev. B **62**, 7956 (2000).

[19] Y. Tanaka, Y. Sakurai, A. T. Stewart, N. Shiotani, P. E. Mijnarends, S. Kaprzyk, and A. Bansil, Phys. Rev. B **63**, 045120 (2001).

[20] J. Kwiatkowska, B. Barbiellini, S. Kaprzyk, A. Bansil, H. Kawata, and N. Shiotani, Phys. Rev. Lett. **96**, 186403 (2006).

[21] G. Oomi, F. Honda, T. Kagayama, F. Itoh, H. Sakurai, H. Kawata, and O. Shimomura, J. Synchrotron Rad. **5**, 932 (1998).

[22] K. Hämäläinen, S. Huotari, J. Laukkanen, A. Soininen, S. Manninen, C.-C. Kao, T. Buslaps, and M. Mezouar, Phys. Rev. B **62**, R735 (2000).

[23] A. A. Sabouri-Dodaran, Ch. Bellin, G. Loupias, M. Marangolo, S. Rabii, F. Rachdi, Th. Buslaps, and M. Mezouar, Phys. Rev. B **72**, 085412 (2005).

[24] J. S. Tse, D. D. Klug, D. T. Jiang, C. Sternemann, M. Volmer, S. Huotari, N. Hiraoka, V. Honkimäki, and K. Hämäläinen, Appl. Phys. Lett. **87**, 191905 (2005).

[25] A. Shukla, B. Barbiellini, A. Erb, A. Manuel, B. Revaz, T. Buslaps, V. Honkimaki, and P. Suortti, J. Phys. Chem. Solids **61**, 357 (2000).

[26] K. Nygård, S. Huotari, K. Hämäläinen, S. Manninen, T. Buslaps, N. Hari Babu, M. Kambara, and D. A. Cardwell, Phys. Rev. B **69**, 020501(R) (2004).

[27] S. B. Dugdale, R. J. Watts, J. Laverock, Zs. Major, M. A. Alam, M. Samsel-Czekala, G. Kontrym-Sznajd, Y. Sakurai, M. Itou, and D. Fort, Phys. Rev. Lett. **96**, 046406 (2006).

[28] C. Sternemann, S. Huotari, M. Hakala, M. Paulus, M. Volmer, C. Gutt, T. Buslaps, N. Hiraoka, D. D. Klug, K. Hämäläinen, M. Tolan, and J. S. Tse, Phys. Rev. B **73**, 195104 (2006).

[29] N. Hiraoka, T. Buslaps, V. Honkimäki, T. Nomura, M. Itou, Y. Sakurai, Z. Q. Mao, and Y. Maeno, Phys. Rev. B. **74**, 100501(R) (2006).

[30] N. Sakai and K. Ôno, Phys. Rev. Lett. **37**, 351 (1976).

[31] M. J. Cooper, S. P. Collins, D. N. Timms, A. Brahmia, P. P. Kane, R. S. Holt, and D. Laundy, Nature **333**, 151 (1988).

[32] K. Das Gupta, Phys. Rev. Lett. **3**, 38 (1959).

[33] C. J. Sparks Jr., Phys. Rev. Lett. **33**, 262 (1974).

[34] W. Schülke, J. Phys.: Condens. Matter **13**, 7557 (2001).

[35] A. Kotani and S. Shin, Rev. Mod. Phys. **73**, 203 (2001).

[36] E. Burkel, Rep. Prog. Phys. **63**, 171 (2000).

[37] T. Scopigno, G. Ruocco, and F. Sette, Rev. Mod. Phys. **77**, 881 (2005).

[38] U. Bergmann, Ph. Wernet, P. Glatzel, M. Cavalleri, L. G. M. Pettersson, A. Nilsson, and S. P. Cramer, Phys. Rev. B **66**, 092107 (2002).

[39] F. Sette, G. Ruocco, M. Krisch, U. Bergmann, C. Masciovecchio, V. Mazzacurati, G. Signorelli, and R. Verbeni, Phys. Rev. Lett. **75**, 850 (1995).

[40] D. Eisenberg and W. Kaufmann, *The Structure and Properties of Water* (Oxford University Press, Oxford, 1969).

[41] F. H. Stillinger, Science **209**, 451 (1980).

[42] B. Guillot, J. Mol. Liquids **101**, 219 (2002).

[43] M. J. Cooper, Rep. Prog. Phys. **48**, 415 (1985).

[44] M. J. Cooper, P. E. Mijnarends, N. Shiotani, N. Sakai, and A. Bansil (eds.), *X-Ray Compton Scattering* (Oxford University Press, Oxford, 2004).

[45] M. J. Puska and R. M. Nieminen, Rev. Mod. Phys. **66**, 841 (1994).

[46] F. Bell and J. R. Schneider, J. Phys.: Condens. Matter **13**, 7905 (2001).

[47] I. E. McCarthy and E. Weigold, Rep. Prog. Phys. **54**, 789 (1991).

[48] T. Head-Gordon and G. Hura, Chem. Rev. **102**, 2651 (2002).

[49] C. J. Fecko, J. D. Eaves, J. J. Loparo, A. Tokmakoff, and P. L. Geissler, Science **301**, 1698 (2003).

[50] K. Modig, B. G. Pfrommer, and B. Halle, Phys. Rev. Lett. **90**, 075502 (2003).

[51] Ph. Wernet, D. Nordlund, U. Bergmann, M. Cavalleri, M. Odelius, H. Ogasawara, L. Å. Näslund, T. K. Hirsch, L. Ojamäe, P. Glatzel, L. G. M. Pettersson, and A. Nilsson, Science **304**, 995 (2004).

[52] I. R. Epstein and A. C. Tanner, in *Compton scattering*, (ed.) B. Williams, 209 (McGraw-Hill, London, 1977).

[53] E. D. Isaacs, A. Shukla, P. M. Platzman, D. R. Hamann, B. Barbiellini, and C. A. Tulk, Phys. Rev. Lett. **82**, 600 (1999).

[54] T. K. Ghanty, V. N. Staroverov, P. R. Koren, and E. R. Davidson, J. Am. Chem. Soc. **122**, 1210 (2000).

[55] A. H. Romero, P. L. Silvestrelli, and M. Parrinello, J. Chem. Phys. **115**, 115 (2001).

[56] S. Ragot, J.-M. Gillet, and P. J. Becker, Phys. Rev. B **65**, 235115 (2002).

[57] M. Hakala, S. Huotari, K. Hämäläinen, S. Manninen, Ph. Wernet, A. Nilsson, and L. G. M. Pettersson, Phys. Rev. B **70**, 125413 (2004).

[58] B. Barbiellini and A. Shukla, Phys. Rev. B **66**, 235101 (2002).

[59] L. Ojamäe and K. Hermansson, J. Phys. Chem. **98**, 4271 (1994).

[60] W. Schülke, in *Handbook on Synchrotron Radiation*, vol. 3, (eds.) G. S. Brown and D. E. Moncton, 565 (Elsevier, Amsterdam, 1991).

[61] W. Schülke, in *X-Ray Compton Scattering*, (eds.) M. J. Cooper, P. E. Mijnarends, N. Shiotani, N. Sakai, and A. Bansil, 22 (Oxford University Press, Oxford, 2004).

[62] P. Fajardo, V. Honkimäki, T. Buslaps, and P. Suortti, Nucl. Instr. Meth. Phys. Res. B **134**, 337 (1998).

[63] L. van Hove, Phys. Rev. **95**, 249 (1954).

[64] P. Eisenberger and P. M. Platzman, Phys. Rev. A **2**, 415 (1970).

[65] R. Ribberfors, Phys. Rev. B **12**, 2067 (1975).

[66] P. Holm, Phys. Rev. A **37**, 3706 (1988).

[67] C. Sternemann, K. Hämäläinen, A. Kaprolat, A. Soininen, G. Döring, C.-C. Kao, S. Manninen, and W. Schülke, Phys. Rev. B **62**, R7687 (2000).

[68] J. A. Soininen, K. Hämäläinen, and S. Manninen, Phys. Rev. B **64**, 125116 (2001).

[69] F. Bell, Phys. Rev. B **67**, 155110 (2003).

[70] A. Issolah, B. Levy, A. Beswick, and G. Loupias, Phys. Rev. A **38**, 4509 (1988).

[71] P. Holm and R. Ribberfors, Phys. Rev. A **40**, 6251 (1989).

[72] A. Issolah, Y. Garreau, B. Lévy, and G. Loupias, Phys. Rev. B **44**, 11029 (1991).

[73] S. Huotari, K. Hämäläinen, S. Manninen, A. Issolah, and M. Marangolo, J. Phys. Chem. Solids **62**, 2205 (2001).

[74] P. Hohenberg and W. Kohn, Phys. Rev. **136**, B864 (1964).

[75] W. Kohn and L. J. Sham, Phys. Rev. **140**, A1133 (1965).

[76] R. G. Parr and W. Yang, *Density-Functional Theory of Atoms and Molecules* (Oxford University Press, Oxford, 1989).

[77] Á. Nagy, Phys. Rep. **298**, 1 (1998).

[78] I. R. Epstein and W. N. Lipscomb, J. Chem. Phys. **53**, 4418 (1970).

[79] P. Duffy, D. P. Chong, M. E. Casida, and D. R. Salahub, Phys. Rev. A **50**, 4707 (1994).

[80] J. R. Hart and A. J. Thakkar, Int. J. Quantum Chem. **102**, 673 (2005).

[81] P. Eisenberger and W. C. Marra, Phys. Rev. Lett. **27**, 1413 (1971).

[82] R. Car and M. Parrinello, Phys. Rev. Lett. **55**, 2471 (1985).

[83] B. Chen, I. Ivanov, M. L. Klein, and M. Parrinello, Phys. Rev. Lett. **91**, 215503 (2003).

[84] StoBe-deMon version 1.0, K. Hermann and L. G. M. Pettersson *et al.*, StoBe Software (2002).

[85] B. Hammer, L. B. Hansen, and J. K. Nørskov, Phys. Rev. B **59**, 7413 (1999).

[86] J. P. Perdew, K. Burke, and M. Ernzerhof, Phys. Rev. Lett. **77**, 3865 (1996).

[87] P. A. M. Dirac, Proc. Cambridge Phil. Soc. **26**, 376 (1930).

[88] S. H. Vosko, L. Wilk, and M. Nusair, Can. J. Phys. **58**, 1200 (1980).

[89] Gaussian 03, M. J. Frisch *et al.*, Gaussian Inc. (2004).

[90] J. P. Perdew and Y. Wang, Phys. Rev. B **45**, 13244 (1992).

[91] J. P. Perdew, J. A. Chevary, S. H. Vosko, K. A. Jackson, M. R. Pederson, D. J. Singh, and C. Fiolhais, Phys. Rev. B **46**, 6671 (1992).

[92] I. Makkonen, M. Hakala, and M. J. Puska, J. Phys. Chem. Solids **66**, 1128 (2005).

[93] G. Kresse and J. Furthmüller, Comput. Mater. Sci. **6**, 15 (1996).

[94] G. Kresse and J. Furthmüller, Phys. Rev. B **54**, 11169 (1996).

[95] P. Suortti, T. Buslaps, P. Fajardo, V. Honkimäki, M. Kretzschmer, U. Lienert, J. E. McCarthy, M. Renier, A. Shukla, T. Tschentscher, and T. Meinander, J. Synchrotron Rad. **6**, 69 (1999).

[96] Y. Sakurai, J. Synchrotron Rad. **5**, 208 (1998).

[97] P. Suortti, T. Buslaps, M. DiMichiel, V. Honkimäki, U. Lienert, J. E. McCarthy, J. M. Merino, and A. Shukla, Nucl. Instr. Meth. Phys. Res. A **467-468**, 1541 (2001).

[98] N. Hiraoka, T. Buslaps, V. Honkimäki, and P. Suortti, J. Synchrotron Rad. **12**, 670 (2005).

[99] A. M. Bebb, J. W. Taylor, J. A. Duffy, Z. F. Banfield, M. J. Cooper, M. R. Lees, J. E. McCarthy, and D. N. Timms, Phys. Rev. B **71**, 024407 (2005).

[100] X.-M. Maréchal, T. Hara, T. Tanabe, T. Tanaka, and H. Kitamura, J. Synchrotron Rad. **5**, 431 (1998).

[101] N. Hiraoka, M. Itou, T. Ohata, M. Mizumaki, Y. Sakurai, and N. Sakai, J. Synchrotron Rad. **8**, 26 (2001).

[102] Y. Sakurai and M. Itou, J. Phys. Chem. Solids **65**, 2061 (2004).

[103] H. Tanaka, T. Aoki, T. Asaka, S. Date, K. Fukami, Y. Furukawa, H. Hanaki, N. Hosoda, T. Kobayashi, N. Kumagai, M. Masaki, T. Masuda *et al.*, in *Proceedings of EPAC 2004*, 222 (Lucerne, 2004).

[104] N. Sakai, J. Phys. Soc. Japan **56**, 2477 (1987).

[105] Y. Kakutani and N. Sakai, J. Phys. Chem. Solids **65**, 2071 (2004).

[106] P. A. Egelstaff, *An Introduction to the Liquid State* (Oxford University Press, Oxford, 1992), 2nd edn.

[107] K. Ichikawa, Y. Kameda, T. Yamaguchi, H. Wakita, and M. Misawa, Mol. Phys. **73**, 79 (1991).

[108] Th. Steiner, Angew. Chem. Int. Ed. **41**, 48 (2002).

[109] J. Korchowiec and T. Uchimaru, J. Chem. Phys. **112**, 1623 (2000).

[110] J.-H. Guo, Y. Luo, A. Augustsson, J.-E. Rubensson, C. Såthe, H. Ågren, H. Siegbahn, and J. Nordgren, Phys. Rev. Lett. **89**, 137402 (2002).

[111] A. Nilsson, H. Ogasawara, M. Cavalleri, D. Nordlund, M. Nyberg, Ph. Wernet, and L. G. M. Pettersson, J. Chem. Phys. **122**, 154505 (2005).

[112] V. F. Petrenko and R. W. Whitworth, *Physics of Ice* (Oxford University Press, Oxford, 1999).

[113] A. K. Soper, Chem. Phys. **258**, 121 (2000).

[114] K. Laasonen, M. Sprik, M. Parrinello, and R. Car, J. Chem. Phys. **99**, 9080 (1993).

[115] B. Hetényi, F. De Angelis, P. Giannozzi, and R. Car, J. Chem. Phys. **120**, 8632 (2004).

[116] J. D. Smith, C. D. Cappa, K. R. Wilson, B. M. Messer, R. C. Cohen, and R. J. Saykally, Science **306**, 851 (2004).

[117] A. K. Soper, J. Phys.: Condens. Matter **17**, S3273 (2005).

[118] D. Xenides, B. R. Randolf, and B. M. Rode, J. Chem. Phys. **122**, 174506 (2005).

[119] M. Odelius, M. Cavalleri, A. Nilsson, and L. G. M. Pettersson, Phys. Rev. B **73**, 024205 (2006).

[120] D. Prendergast and G. Galli, Phys. Rev. Lett. **96**, 215502 (2006).

[121] T. Head-Gordon and M. E. Johnson, Proc. Natl. Acad. Sci. USA **103**, 7973 (2006).

[122] M. Leetmaa, M. Ljungberg, H. Ogasawara, M. Odelius, L.-Å. Näslund, A. Nilsson, and L. G. M. Pettersson, J. Chem. Phys. **125**, 244510 (2007).

[123] T. S. Pennanen, J. Vaara, P. Lantto, A. J. Sillanpää, K. Laasonen, and J. Jokisaari, J. Am. Chem. Soc. **126**, 11093 (2004).

[124] Th. Steiner and W. Saenger, Acta. Cryst. B **50**, 348 (1994).

[125] H. F. J. Savage and J. L. Finney, Nature **322**, 717 (1986).

[126] A. G. Császár, G. Czakó, T. Furtenbacher, J. Tennyson, V. Szalay, S. V. Shirin, N. F. Zobov, and O. L. Polyansky, J. Chem. Phys. **122**, 214305 (2005).

[127] B. Tomberli, C. J. Benmore, P. A. Egelstaff, J. Neuefeind, and V. Honkimäki, J. Phys.: Condens. Matter **12**, 2597 (2000).

[128] Y. S. Badyal, D. L. Price, M.-L. Saboungi, D. R. Haeffner, and S. D. Shastri, J. Chem. Phys. **116**, 10833 (2002).

[129] R. T. Hart, C. J. Benmore, J. Neuefeind, S. Kohara, B. Tomberli, and P. A. Egelstaff, Phys. Rev. Lett. **94**, 047801 (2005).

[130] R. A. Kuharski and P. J. Rossky, J. Chem. Phys. **82**, 5164 (1985).

[131] L. Bosio, S.-W. Chen, and J. Teixeira, Phys. Rev. A **27**, 1468 (1983).

[132] R. D. Davy and M. B. Hall, Inorg. Chem. **27**, 1417 (1988).

[133] A. W. Omta, M. F. Kropman, S. Woutersen, and H. J. Bakker, Science **301**, 347 (2003).

[134] A. H. Narten, F. Vaslow, and H. A. Levy, J. Chem. Phys. **11**, 5017 (1973).

[135] Y. Marcus, Chem. Rev. **88**, 1475 (1988).

[136] H. Ohtaki and T. Radnai, Chem. Rev. **93**, 1157 (1993).

[137] M. Patra and M. Karttunen, J. Comput. Chem. **25**, 678 (2004).